SUPPLEMENTARY MATERIALS

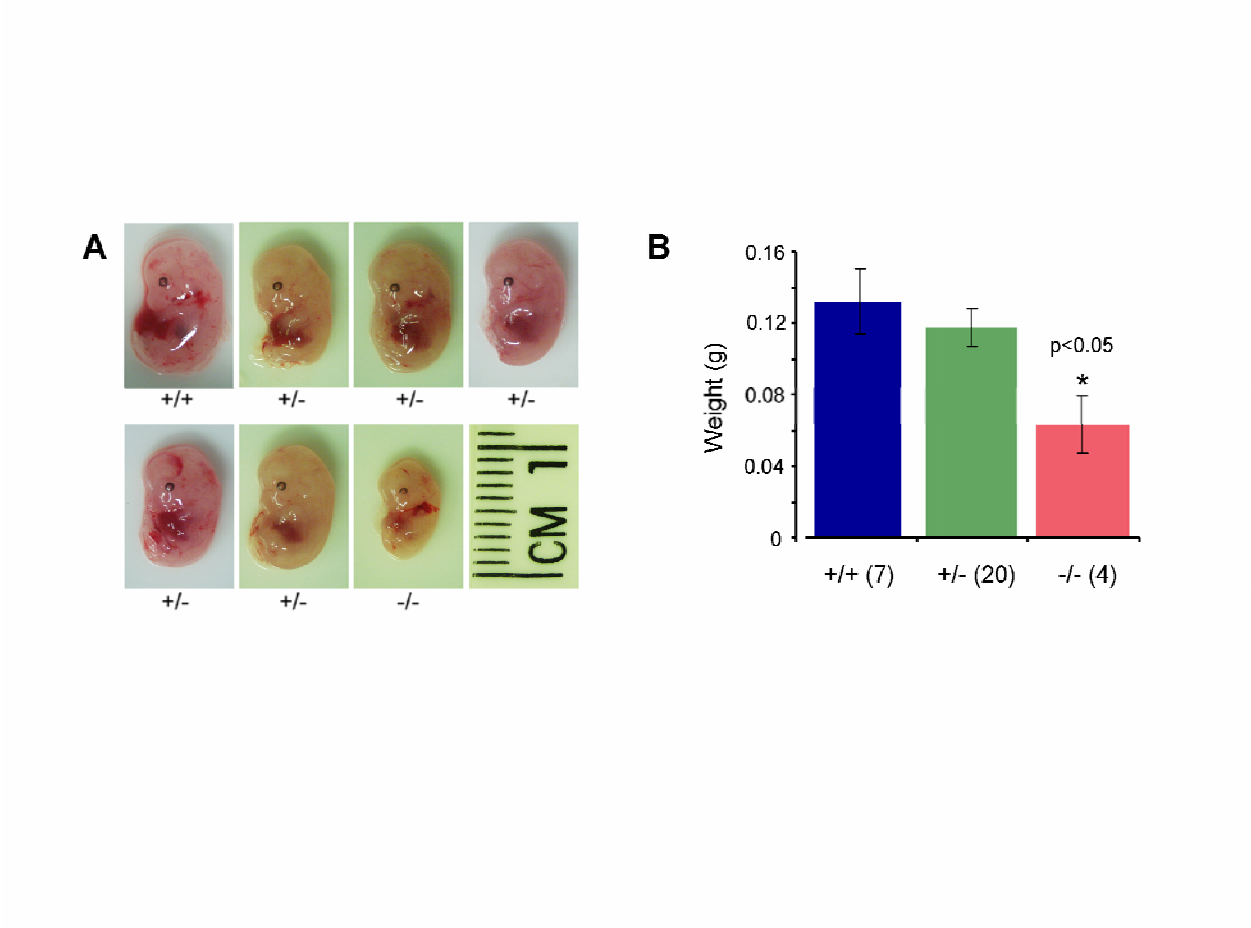

Figure S1. MMRRC *Nedd4* KO animals are growth retarded. A, 13.5 dpc animals from a single litter with their Nedd4 genotypes are shown. **B,** Body weights of 13.5 dpc *Nedd4* +/+, +/- and -/- embryos. The number of animals for each genotype are shown in parenthesis. Error bars represent SEM.

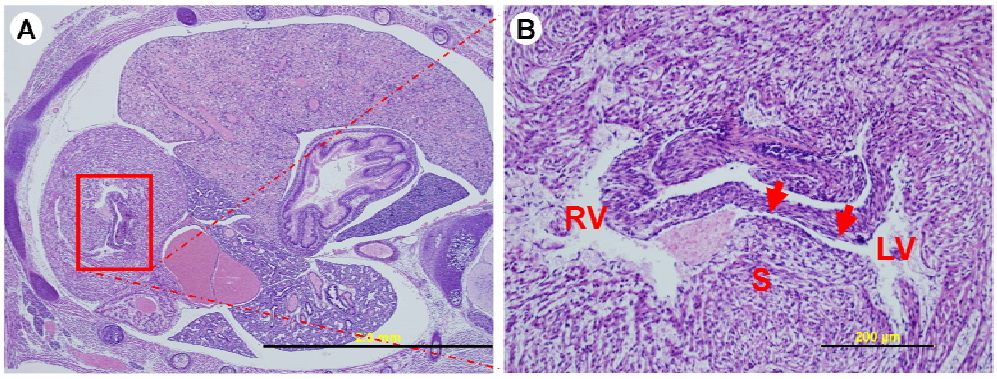

Fig. S2. Some *Nedd4*$^{-/-}$ embryos have ventricular septal defect (VSD). Sections from late gestation embryos were examined. Membranous VSD (arrows) was found in 1 out of 3 *Nedd4* -/- embryos. LV: left ventricle. RV: right ventricle. S: septum. Scale bar: 2 mm (panel **A**) and 200 μm (panel **B**).

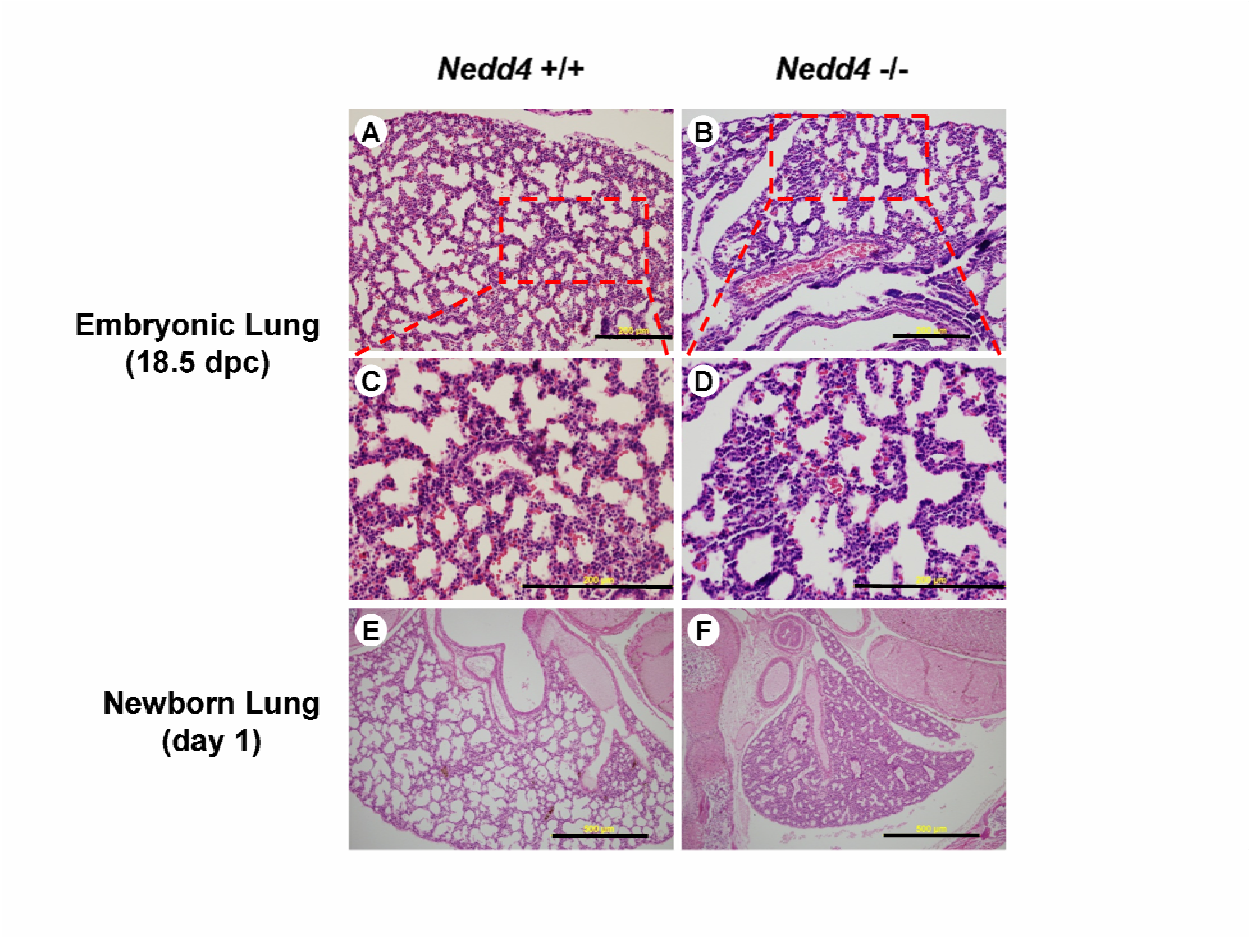

Fig. S3. Normal lung development in *Nedd4*$^{-/-}$ embryos. Lungs were taken from E18.5 embryos (**A**-**D**) and postnatal day 1 mice (**E** and **F**), and processed for histology (hematoxylin and eosin staining). Wild-type littermates were used as controls. More than 4 mice were used for each genotype and typical histology is shown. The homozygous mutant mouse lungs (**B**, **D** and **F**) had fewer alveoli than their wild type counterparts (**A**, **C** and **E**), but the overall lung structure was similar. The low magnification (x 100) photomicrograph of the lung from a newborn homozygous mutant animal (**F**), shows marked reduction in lung size and little evidence of aeration (compare to wild-type lung in which alveoli are clearly expanded). Scale bar 200 μm (panels **A**-**D**) and 500 μm (panels **E**-**F**).

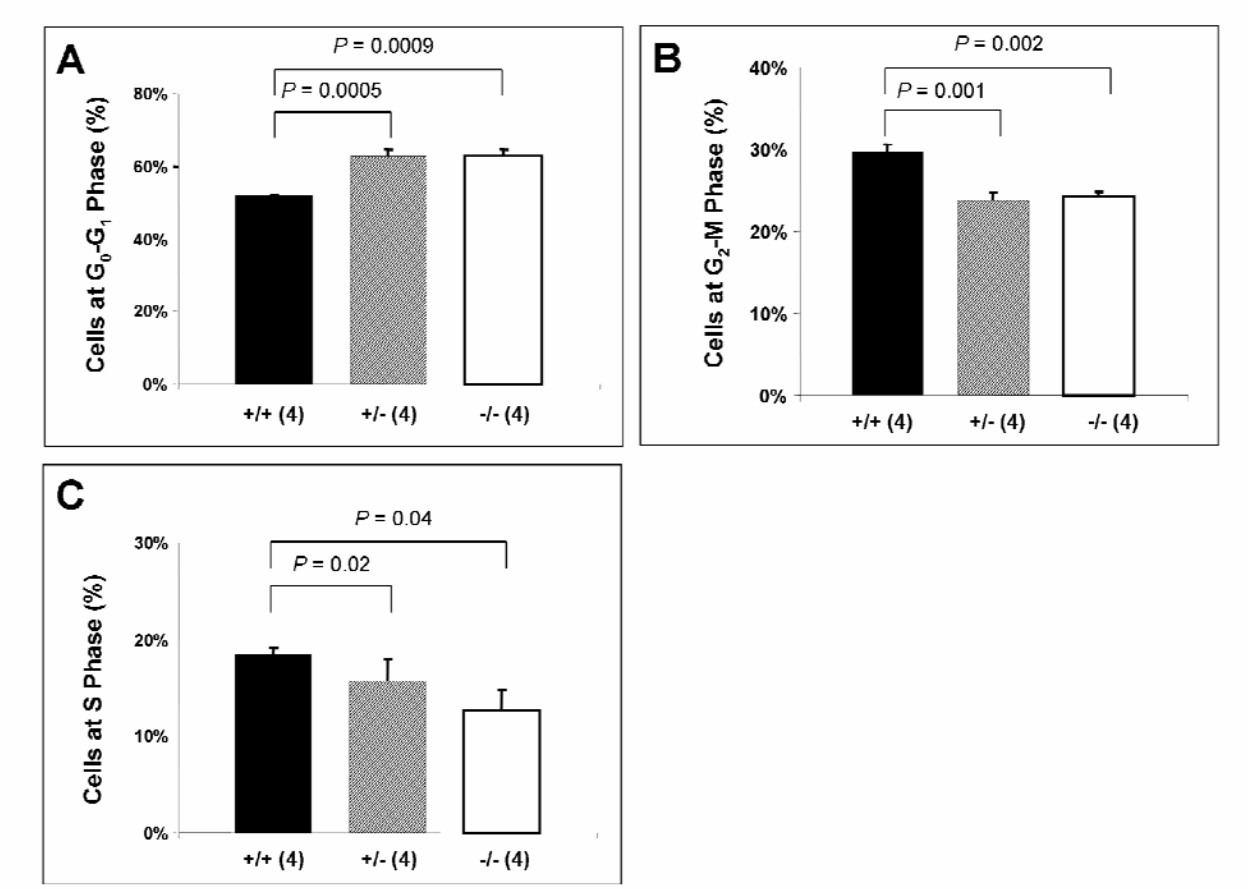

Fig. S4. Mouse embryonic fibroblasts isolated from both *Nedd4*$^{+/-}$ and *Nedd4*$^{-/-}$ embryos show growth arrest at G0-G1 phase of the cell cycle. Cell cycle information was obtained using passage number-matched asynchronous MEFs (passage numbers 2 to 5) under normal culture conditions (DMEM + 10%FCS). Cells were stained with PI (propidium iodide) and treated with RNase A to remove cytoplasmic RNA. Stained cells were sorted based on DNA content. Both *Nedd4* +/+ and -/- cells accumulated in the G0/G1 phases. The differences between *Nedd4* +/+ and +/- and between +/+ and -/- were significant (panel **A**). Accordingly, the percentages of cells in G2-M and S phases decreased in the cases of the Nedd4 +/- and -/- cells

(panels **B** and **C**). The number of independent experiments is shown in parenthesis, and P values indicating significance of differences are also indicated.

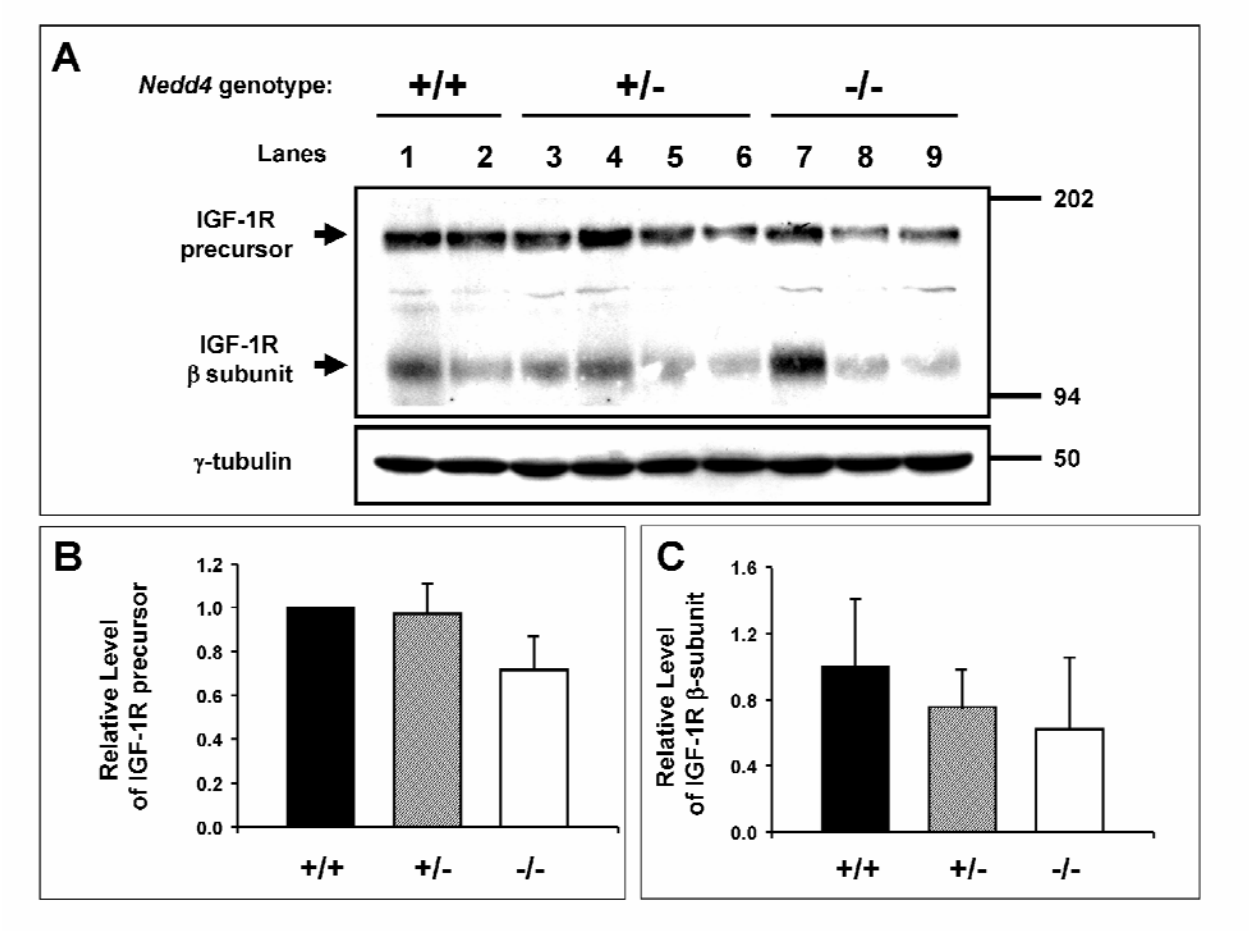

Fig. S5. Total cellular levels of the IGF-1R precursor and the processed β subunit do not vary consistently with *Nedd4* gene dosage. Mouse embryo fibroblast cultures generated from individual embryos were grown in DMEM + 10% FBS. (**A**) At *in vitro* passage 1, subconfluent cultures were harvested in 0.5% Triton X-100 lysis buffer. Each gel lane was loaded with 100 μg of postnuclear supernatant protein. Following transfer to PVDF membranes, the cellular proteins were probed with anti-IGF-1R-β antibody (1:1,000 dilution); both the IGF-1R precursor and the mature β subunit were detected (band size for each indicated by arrows). The γ-tubulin immunoblot signals

serve as the protein loading control. Results for levels of both the precursor (**B**) and the β subunit (**C**) were quantified.

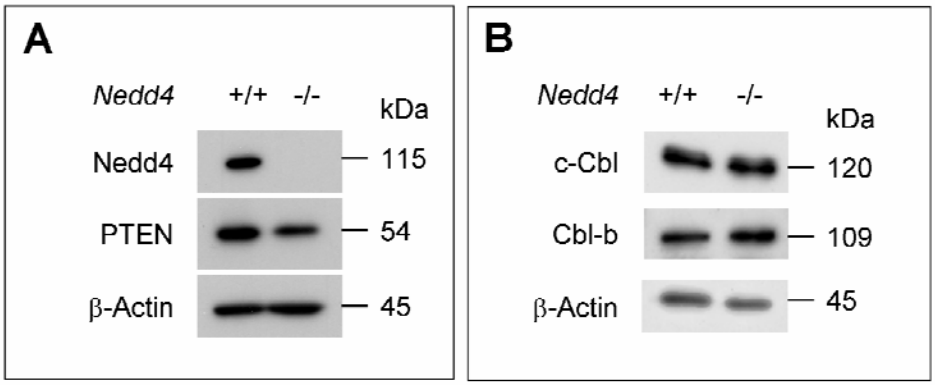

Fig. S6. Cellular PTEN, c-Cbl, and Cbl-b levels are not significantly different in *Nedd4*$^{-/-}$ MEFs. The levels of (**A**) PTEN and (**B**) c-Cbl and Cbl-b in MEFs were assessed by immunoblotting. The MEF genotypes were confirmed by the presence and absence of Nedd4 protein. The actin immunoblot signals serve as protein loading controls. The Nedd4 and actin blots shown here are same as in Figure 7I, because the data for PTEN were derived from the same samples.

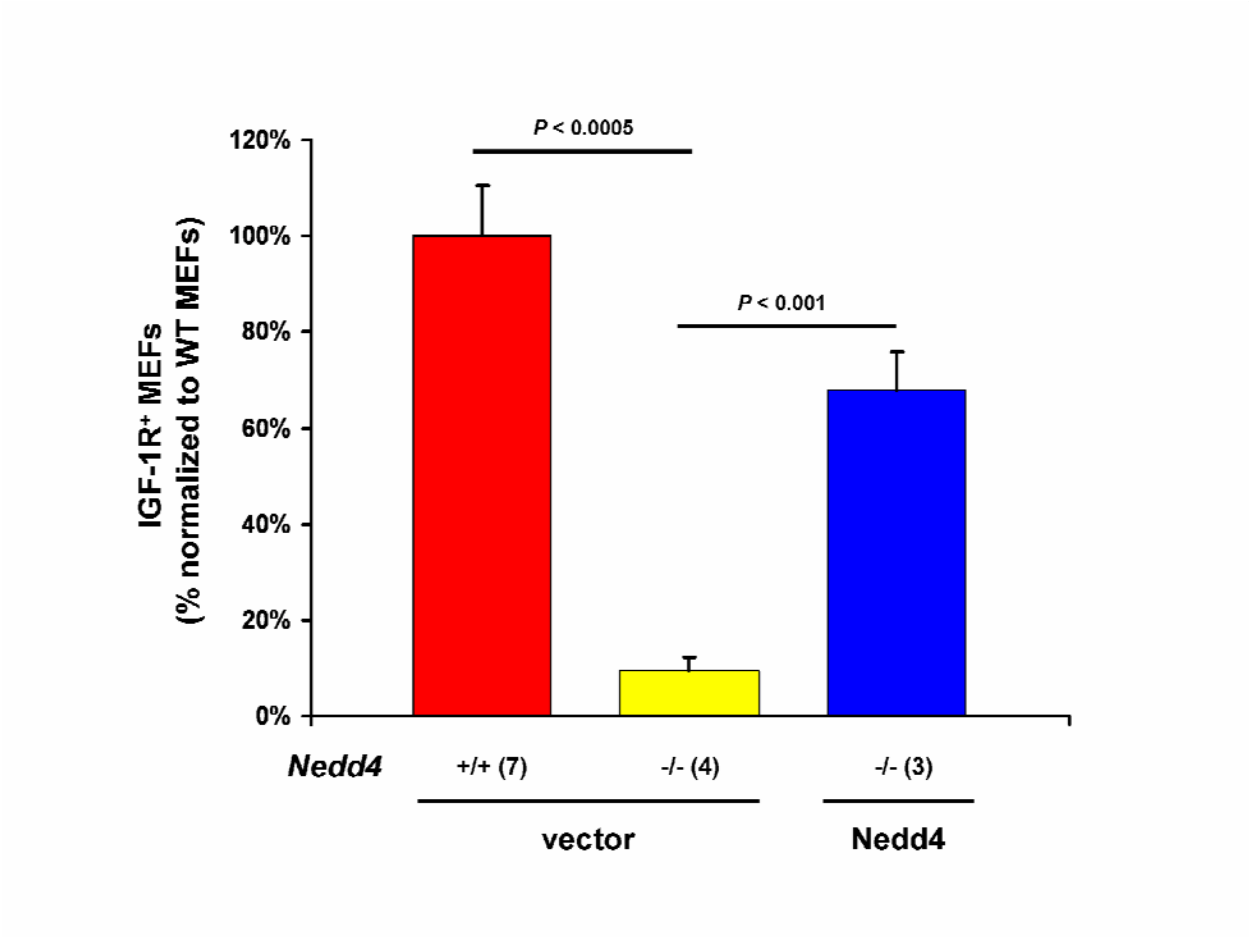

Fig. S7. Re-expression of Nedd4 in *Nedd4*$^{-/-}$ MEFs restores IGF-1R to the cell surface. A Nedd4 expression vector or empty vector was transiently transfected in MEFs as indicated. Fluorescein isothiocyantate (FITC)-conjugated IGF-1Rα antibody was used to label IGF-1R-positive cells. Sorting of IGF-1R-positive cells was carried out with a LSR flow cytometer and analyzed with CELLQUEST software (BD Biosciences, San Jose, CA). The number of independent experiments is shown in parenthesis, and P values indicating significance of differences are also indicated.

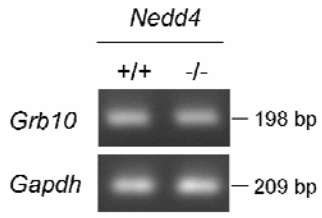

Figure S8. Similar levels of *Grb10* transcript in *Nedd4*$^{+/+}$ and *Nedd4*$^{-/-}$ MEFs. RT-PCR was performed on cDNA prepared from RNA isolated from MEFs. PCR (30 cycles) were carried out using appropriate primers, including *Gapdh* as a control. Expected sizes for *Grb10* and *Gapdh* PCR DNA products are shown. 25 cycles of PCR showed similar results.

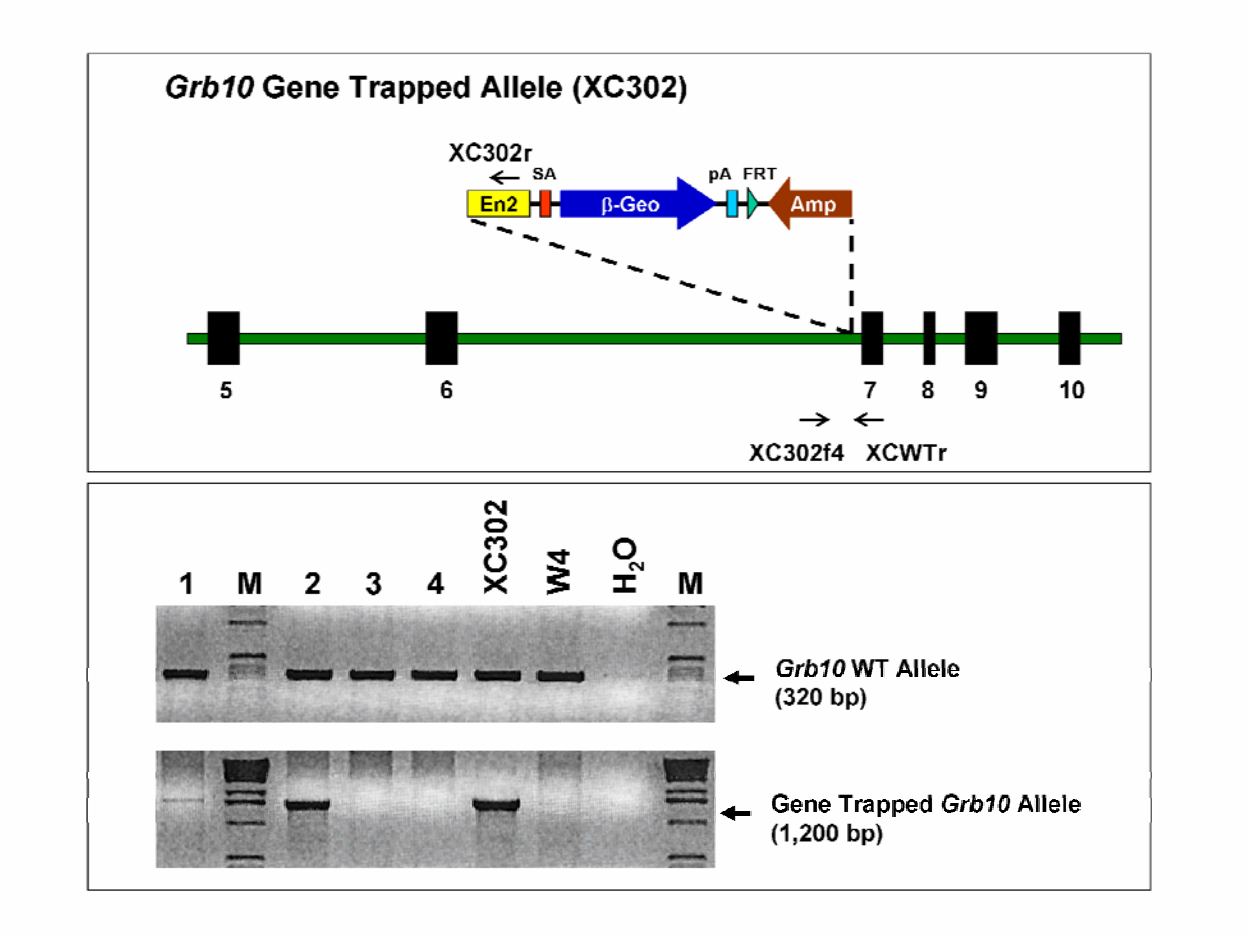

Fig. S9. Generation and genotyping of *Grb10*-deficient mice. Upper panel: schematic representation of the genomic structure of the *Grb10* gene, from exons 5 to 10. The gene-trapping vector was inserted into the 3' end of intron 6, which is less than 200 bp from the exon 7. The arrows indicate locations and directions of the PCR primers (located within intron 6, exon 7 and the En2 sequence) that were used for genotyping. Lower panel: typical PCR genotyping of a litter of 4 mice. XC302 and W4 are gene-trapped and wild-type ES cells, respectively, that were used as controls.

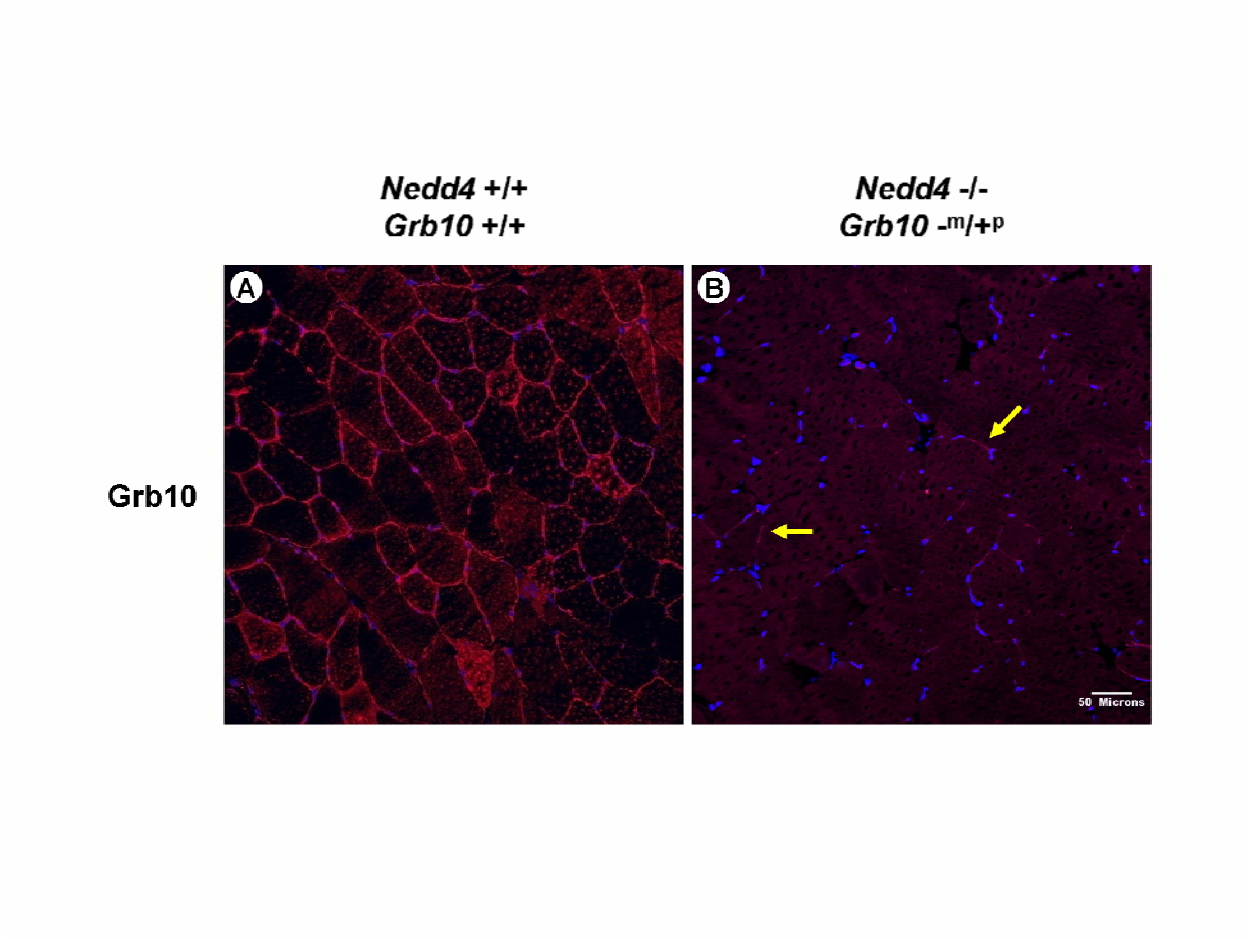

Fig. S10. Paternally inherited *Grb10* allele is expressed at low levels in muscle. Biopsies from tibias anterior muscle were obtained from wild-type (**A**) and *Nedd4*$^{-/-}$;*Grb10*$^{+/-}$ mice (**B**). Immunohistochemistry with rabbit anti-mouse Grb10 antibody (Santa Cruz Biotech, Santa Cruz, CA) was performed on frozen muscle sections. Positive signals were visualized with Alexa Fluor 488-conjugated goat anti-rabbit IgG (red). Nuclei were stained with ToPro-3 (blue). Arrows in panel **B** indicate portions of the membrane that are positive for Grb10. Scale bar 50 μm.